The role of TRPC channels in Ca^{2+} dyshomeostasis in Malignant Hyperthermia

Jose R Lopez M.D., Ph.D[1,2,#], Vikas Kaura M.D.[3,#], Phillip Hopkins M.D[4], Xiaochen Liu Ph.D[4], Arkady Uryach M.D., Ph.D[3], Jose Adams M.D.[3,] Paul D Allen M.D., Ph.D[1,4]

[1] Department of Molecular Biosciences, School of Veterinary Medicine, University of California at Davis, Davis, CA 95616

[2] Department of Research, Mount Sinai, Medical Center, Miami, FL 33140, USA

[3]Division of Neonatology, Mount Sinai Medical Center, Miami, FL 33140, USA

[4] Malignant Hyperthermia Investigation Unit, St James' University Hospital, Leeds, United Kingdom.

[#]These authors had equal contributions to the work.
Corresponding Author: Paul D Allen, Malignant Hyperthermia Investigation Unit, St James' University Hospital, Leeds, United Kingdom, Email: p.d.allen@leeds.ac.uk

Clinial Trial Number (not applicable)

Prior Presentations: Presented in part as a poster at the 63rd Annual Meeting of the Biophysical Society, Baltimore Maryland, March 2-6, 2019

Word and Element Counts: Number of words in Abstract **290**, in Introduction **493**, and in Discussion **995**; number of figures **8**; number of tables None; number of appendices None; and number of supplementary files None

Running Title: **The role of TRPC channels in MH**

Summary Statement: (not applicable)

Funding Statement: National Institute of Arthritis, Musculoskeletal and Skin Diseases (1R01AR068897-01A1; P.D.A., P.M.H., J.R.L., X.L.); National Institute of Arthritis, Musculoskeletal and Skin Diseases (2P01 AR-05235; P.D.A., J.R. L., P.M.H.); Medical Research Council (MR/N002407/1; V.K., P.M.H., P.D.A.), AFM-Téléthon-France (21543; J.R.L.)

Conflicts of Interest The authors declare that they have no conflicts of interest with the contents of this article[1]

[1] The content is solely the responsibility of the authors and does not necessarily represent the official views of the National Institutes of Health or the Medical Research Council

Abstract.-

Background: Until recently, the mechanism for the malignant hyperthermia (MH) crisis has been attributed solely to sustained massive Ca^{2+} release from the sarcoplasmic reticulum on exposure to triggering agents. We now investigate the role of TRPC channels as an important contributor to the Ca^{2+} dyshomeostasis observed in MH.

Methods: We examined the mechanisms responsible for Ca^{2+} dyshomeostasis in *RYR1*-pG2435R MH muscle cells using ion selective microelectrodes, Mn^{2+} quench of Fura2 fluorescence, and western blots.

Results: *RYR1*-pG2435R MH mouse muscle cells show gene dose-dependent increases in both $[Ca^{2+}]_i$ and $[Na^+]_i$ and the rate of Mn^{2+} quench on exposure to TRPC3/6 activators oleoyl-acyl-sn-glycerol. These increases were inhibited by *i)* removal of extracellular Ca^{2+} *ii)* the nonspecific sarcolemmal cation entry blocker, Gd^{3+} or *iii)* SAR7334, which specifically blocks TRPC6 and TRPC3 mediated cation influx. Furthermore, local pretreatment with SAR7334 partially decreased the elevation of $[Ca^{2+}]_i$ that is seen in MH muscles during exposure to isoflurane. Western blot analysis showed that expression of TRPC3, TRPC6 channels was significantly increased in G2435R muscles in a gene dose-dependent manner, supporting their being the primary molecular basis for increased sarcolemmal cation influx.

Conclusions: Muscle and muscle cells in knock-in mice expressing the *RYR1*-pG2435R mutation are hypersensitive to TRPC3/6 activators oleoyl-acyl-sn-glycerol and hyperforin: this hypersensitivity can be negated with pharmacologic agents that block TRPC3/6 activity. This reinforces our working hypothesis that TRPC channels play a critical role in causing intracellular Ca^{2+} and Na^+ overload in MH susceptible muscle,

both at rest and during the MH crisis.

Introduction.-

Malignant hyperthermia (MH) is an autosomal dominant hypermetabolic condition triggered by volatile anesthetics and depolarizing neuromuscular blockers[1]. The MH crisis is characterized by hypercapnia, tachycardia, hypoxemia, muscle rigidity, hypermetabolism, respiratory and metabolic acidosis and hyperthermia. Human malignant hyperthermia susceptible individuals appear to for the most part remain subclinical until challenged with pharmacologic triggering agents[1-3]. Once the syndrome is triggered, if left untreated, the mortality of a fulminant MH episode is >70%, but availability of dantrolene has reduced the mortality to <8%[1,2]. Molecular genetic studies have established that the type 1 ryanodine receptor gene (*RYR1*) encoding the skeletal muscle sarcoplasmic reticulum (SR) Ca^{2+} release channel as the primary locus for MH[3-6]. More than 200 *RYR1* mutations found throughout the gene have been associated with MH[6]. To date, one spontaneously occurring porcine model (R615C) and 4 murine knock-in models expressing the murine equivalent of human (R163C[7], Y522S[8], G2434R[9] and T4826I[10] MH *RYR1* mutations have been studied in detail. All 5 models exhibit fulminant anesthetic--triggered MH episodes and heat intolerance with varying gene dose relationships. The G2435R variant which is the focus of this study is a model for the most frequent variant associated with MH in the UK and North America. In addition, this is the most common RYR1 variant to be associated with familial genotype-phenotype discordance[11]. It is associated with a relatively weak IVCT phenotype and is less likely to be associated with an elevated serum CK compared with T4826I and R163C[12,13].

The exact molecular mechanisms by which *RYR1* mutations confer MH

susceptibility are unknown. A common characteristic of muscle expressing MH-RyR1 mutations compared to non-susceptible muscle is an increased resting intracellular Ca^{2+} concentration ($[Ca^{2+}]_i$) in humans[14] and animal models[15-18]. We have shown that exposure to halothane or isoflurane at clinically relevant concentrations causes $[Ca^{2+}]_i$ to rise several fold in MH muscle in one porcine and three murine experimental models, whereas exposure to the same concentrations of halothane or isoflurane had no effect in non-susceptible muscle[17,19,20].

Until recently, the mechanism for the MH crisis has been attributed solely to massive self-sustaining release of Ca^{2+} from the SR on exposure to triggering agents. Counter to this view, we have introduced a new paradigm that implicates nonspecific sarcolemmal cation entry channels as both the predominant source of acutely elevated intracellular calcium and sodium during fulminant MH and are significant contributors to chronically elevated $[Ca^{2+}]_i$ and $[Na^+]_i$ in quiescent MH-susceptible muscles[21,22].

The objective of the current study was to test the hypothesis that TRPCs play a major role in the Ca^{2+} dyshomeostasis that we recently described in a *RYR1* pG2435R knock-in murine model of MH[9] and which were similar to our previous observations in the *RYR1* pR163C mouse[21,22]. Here, we use newly available more specific pharmacologic agents to probe TRPC function allowing us to determine their importance in initiating and supporting the MH crisis in response to triggering agents.

Material and Methods.-

Animals

Animals used in this study were housed in pathogen-free conditions with free access to food, water and 12 hr light-and-dark cycles. All experiments were undertaken with either UK Home Office, University of California at Davis IACUC or Mount Sinai Hospital IACUC approval. For single fiber and *in vivo* studies a mixture of male and female mice between 12-16 weeks were used and for myotube studies, myoblasts were isolated from 10-12 day old neonatal mice. All experiments were terminal. For *in vivo* experiments the MH animals were allowed to succumb to isoflurane anesthesia when this was used, otherwise they and all WT animals were euthanized under anesthesia by cervical dislocation. For muscle collection, MH and WT animals were euthanized by cervical dislocation immediately prior to dissection. Because HOM animals were viable, animals were obtained and allocated to HOM and HET experimental groups by selective breeding of HOM females to either HOM or WT C57BL/6J and animals were used as available in the breeding colony when they reached the appropriate age. Studies on WT mice were done on 3-5-month-old C57BL/6J animals purchased from Charles River Laboratories (Wilmington MA) or the St. James's animal facility (Leeds, UK) as needed.

Experimental Preparation

Experiments were conducted at room temperature (~23ºC): (i) *in vitro* using Flexor digitorum brevis (FDB) muscle fibers from 3-5-month-old C57BL/6J (WT), heterozygous MH-G2435R (MH-HET) and homozygous MH-G2435R (MH-HOM) mice. Single fibers were obtained by enzymatic digestion as described previously[21]. (ii) *in vivo*,

in *vastus lateralis* fibers in WT and MH mice anesthetized with ketamine/xylazine (100/5 mg/kg body weight) as described previously[22]. (iii) *in vitro* using myotubes differentiated from myoblasts from C57BL/6 (WT), heterozygous MH-p.G2435R (MH-HET), and homozygous MH-p.G2435R (MH-HOM) mice as described in detail previously[9].

Ca^{2+} and Na^{+} selective microelectrodes

Double-barreled Ca^{2+} and Na^{+} selective microelectrodes were prepared as described previously[14,22]. Each ion-selective microelectrode was individually calibrated before and after the determination of intracellular Ca^{2+} concentration ($[Ca^{2+}]_i$) and intracellular Na^{+} concentration ($[Na^{+}]_i$) as described before[22]. Only those Ca^{2+} selective microelectrodes with a linear relationship between pCa 3 and 7 (Nernstian response, 29.5 and 30.5 mV/pCa unit at 23°C and 37°C, respectively) were used experimentally. The Na^{+} selective microelectrodes gave virtually Nernstian responses at free $[Na^{+}]_e$ between 100 and 10 mM. However, although at concentrations between 10 and 1 mM $[Na^{+}]_e$, the electrodes had a sub-Nernstian response (40–45 mV), their response was of a sufficient amplitude to be able to measure $[Na^{+}]_i$. The sensitivity and response of the Ca^{2+} and Na^{+} selective microelectrodes were not directly affected by any of the drugs used in the present study.

Ca^{2+} and Na^{+} determinations in muscle fibers

Microelectrode recordings were performed as described previously[22]. Single isolated adult *flexor digitorum brevis* muscle fibers (*in vitro*) or *vastus lateralis* muscle fibers (*in vivo*) from WT and MH mice were impaled with either double-barreled Ca^{2+} - or double- barreled Na^{+} -selective microelectrodes, and their potentials were recorded via a high-impedance amplifier (WPI Duo 773 electrometer; WPI, Sarasota, FL, USA). The

potential from the 3 M KCl microelectrode (Vm) was subtracted electronically from either the potential of the Ca^{2+} electrode (V_{CaE}) or the Na^{+} electrode (V_{NaE}) to produce a differential Ca^{2+}- specific potential (V_{Ca}) or Na^{+} -specific potential (V_{Na}) that represents the $[Ca^{2+}]_i$ or $[Na^{+}]_i$, respectively. Vm, V_{Ca}, V_{Na} were filtered (30–50 kHz) to improve the signal-to-noise ratio and stored in a computer for further analysis. Data from any given electrode impalement were accepted if Vm was >or = to -80mV, and if it was possible to make a stable recording of either Vm and V_{Ca}, or Vm and V_{Na} for 60 seconds. These criteria resulted in rejection of data from 20% of *in vivo* impalements and 30-35% of *in vitro* impalements.

Measurements of Mn^{2+} quench of Fura 2 in myotubes and isolated single fibers.

When the Ca^{2+} indicator Fura2 is exposed to Mn^{2+} its fluorescence at its isobestic emission wavelength is quenched. Because TRPC, Orai and slow voltage gated Ca^{2+} channels are permeable to Mn^{2+} as well as Ca^{2+}, the rate of Mn^{2+} quench can be used to determine the rate of Ca^{2+} entry into a cell.

We used Mn^{2+} quench to assess sarcolemmal divalent cation entry in myotubes or isolated single adult muscle fibers loaded with 5 μM Fura2-AM for 30 mins at 37°C. The solution containing the Fura2-AM was washed off and the cells maintained for 25 mins at room temperature to allow de-esterification and equilibration of the intracellular Fura-2. The cells were observed through a 40x 1.3 NA objective on a Nikon Eclipse T2000 epifluorescence microscope using an excitation wave-length of 360+/-5 nm (the isosbestic wavelength of Fura-2 where the fluorescence of the dye is independent of the Ca^{2+} free versus Ca^{2+} bound state), and the emission signal measured at 510+/-40 nm. Images were captured with 2x2 binning at a rate of 5 fps using an intensified 12-bit

digital intensified charge-coupled device (ORCA-ER) and IPLab software. Regions of interest in individual cells were analysed using Image J software (NHLBI), with the data exported to GraphPad Prism 7. Prism was used to fit linear regression models (y=mx+c) for the basal signal in imaging buffer, and then independently in Mn^{2+}-containing solutions with and without treatment drugs. The specific rate of Fura-2 quenching induced by Mn^{2+} entry was calculated by subtracting the basal slope of decline of fluorescence over time from the slope during the application of Mn^{2+} buffer (i.e. net slope) and is expressed as arbitrary fluorescence units (AFU) per second. The net slope was calculated in the absence and presence of treatment drugs. Cells with a positive net slope following the addition of Mn^{2+} buffer were excluded from analysis because this indicated a technical problem with the measurement, for the same reason the slope of the quench signal was normalised to zero when the net slope was positive following treatment with a cation channel antagonist.

Western blot analysis of TRPC3 and TRPC6 expression.-

Gastrocnemius muscles from all genotypes were dissected, minced, and homogenized in modified radioimmunoassay precipitation assay (RIPA) buffer. Total protein concentration was determined using the bicinchoninic acid (BCA) method (Thermo-Scientific, MA, USA). Samples of whole gastrocnemius homogenate were prepared as described by Altamirano et al. [18] and incubated overnight at 4°C with primary antibodies: rabbit anti -TRPC3, dilution 1:2500 (ab51560; Abcam, MA, USA), rabbit anti -TRPC6, dilution 1:2500 (ab62461, Abcam, MA, USA), human anti-actin, dilution of 1:5000 (SC8432; Santa Cruz, CA, USA). All of these antibodies have been validated previously by different research groups and our laboratory. The resolved

bands were detected with a Storm 860 Imaging System (GE Bio-Sciences, NJ, USA). Protein levels were quantified using myImageAnalysis software (Thermo-Fisher Scientific, MA, USA) and normalized to b-actin.

Solutions

The mammalian Ringer solution used for experiments using muscle fibers had the following composition (in mM): 140 NaCl, 5 KCl, 2 $CaCl_2$, 1 $MgCl_2$, 5 glucose, and 10 HEPES, pH 7.4. The imaging buffer used for the experiments with myotubes contained (in mM): 133 NaCl, 5 KCl, 2 $CaCl_2$, 1 $MgCl_2$, 5.5 glucose, and 10 HEPES, pH 7.4. In the Mn^{2+} buffer the $CaCl_2$ and $MgCl_2$ were substituted with 0.5 mM $MnCl_2$. The Ca^{2+} free solution had the following composition (in mM): 140 NaCl, 5 KCl, 2 Mg Cl_2, 1 EGTA, 5 glucose, and 10 HEPES, pH 7.4. 1-oleoyl-2-acetyl-*sn*-glycerol, Gd^{3+}, SAR7334 and hyperforin solutions were made by adding the desired concentration of the reagent to the physiological or Mn^{2+} containing solutions.

Statistics

Neither randomization nor blinding of the investigator performing the test were used for these studies. No specific power calculation was conducted prior to experimentation but the rationale for the sample sizes used was based on our previous studies using this and other animal models of MH with the same and different pharmacologic interventions. All values of intracellular ion concentrations are expressed as mean±SD, with *N* representing the number of mice used for the *in vivo* experiments, and n representing the number of myotubes or muscle fibers in which measurements were carried out. Statistical analysis for studies done on muscle fibers both *in vitro* and *in vivo* was performed using 1-way between genotypes ANOVA with Tukey's post-test

for multiple measurements to determine significance. Normal distribution of the data was verified by histogram analysis. For studies of Mn^{2+} quench in myotubes, the results were not normally distributed, and as a result are expressed as the median±interquartile range. These results were analyzed using a Kruskal-Wallis test with Dunn's multiple comparison to determine significance. $p<0.05$ was accepted as the minimum confidence level for significance for all comparisons but the P values obtained for each comparison are reported. With the exception of the myotube Mn^{2+} quench studies, where positive quench data were excluded or normalized to zero as described above, and muscle fiber data where the criteria for a successful measurement was not met (based on either a depolarized membrane potential or lack of stable electrode recording for 60 seconds), no outlying data were removed from the data collected prior to or after analysis.

Results.-

Resting $[Ca^{2+}]_i$ and $[Na^+]_i$

Malignant hyperthermia is characterized by an intracellular Ca^{2+} and Na^+ dyshomeostasis[14,19,22,23]. Consequently, $[Ca^{2+}]_i$ or $[Na^+]_i$ was measured in quiescent single muscle fibers isolated from WT, MH-HET, and MH-HOM cells using double-barreled ion-specific microelectrodes. $[Ca^{2+}]_i$ was 120±2 nM (n=8) in WT, while it was 156±11 nM (n=11) in HET, and 275±15 nM (n=10) in HOM (p <0.001 for both) (Figure 1A). No statistically significant difference was noted in the resting membrane potential among WT and MH-HET or MH-HOM muscle fibers. Likewise, $[Na^+]_i$ was more elevated in HET, and HOM fibers than that observed in WT fibers. $[Na^+]_i$ was 8±0.1 mM (n=8) in WT fibers, while it was 10±1 mM (n=9) in MH-HET and 14±0.6 mM (n=11) in MH-HOM respectively (p <0.001 for both) (Figure 1A).

As previously reported similar differences for $[Ca^{2+}]_i$ and $[Na^+]_i$ were obtained in the *in-vivo* measurements carried out on the *vastus lateralis* from WT and MH mice[9]. In a new data set carried out for this study $[Ca^{2+}]_i$ in WT was 122±3 nM (n=15) compared to 144±9 nM (n=14) and 259±31 nM (n=18) in MH-HET and MH-HOM muscles respectively (Figure 1B). $[Na^+]_i$ was 8±0.1 mM (n=16) in WT compared to 9.5±1 mM (n=16) and 12.9±1.5 mM (n=13) in MH-HET and MH-HOM fibers respectively(p <0.001 compared to WT) (Figure 1B).

Taken together, the results demonstrate that there is a comparable intracellular Ca^{2+} and Na^+ overload in both isolated *RYR1*-p.G2435R muscle cells and intact muscle fibers compared to WT and that resting intracellular ion recordings under *in vitro* conditions recapitulate those found *in vivo.*

1-oleoyl-2-acetyl-sn-glycerol (OAG) induces an elevation of $[Ca^{2+}]_i$ and $[Na^+]_i$

To directly investigate the effect of diacylglycerol (DAG) on $[Ca^{2+}]_i$ and $[Na^+]_i$ single muscle fibers were exposed to OAG, a membrane-permeable diacylglycerol analog which has been shown to activate transient receptor potential cation channel subfamily C, member 3 (TRPC3) and member 6 (TRPC6) channels[24]. Incubation of muscle fibers in OAG (100 μM) for 5 minutes produces an elevation of $[Ca^{2+}]_i$ in all genotypes. In WT $[Ca^{2+}]_i$ was increased by 60% (from 123±3 nM (n=11) to 196±27 nM (n=13) p<0.001), in MH-HETs it was enhanced by 99% (from 153±11 nM (n=12) to 304±45 nM (n=11) p<0.001) and in MH-HOMs it was elevated by 113% (from 251±25 nM (n=12) to 534±64 nM (n=13) p<0.001) (Figure 2A).

Since the permeability of TRPCs is cation specific but not Ca^{2+} specific, their activation could also increase Na^+ entry and $[Na^+]_i$. Application of OAG (100μM) significantly elevated $[Na^+]_i$ in all genotypes but its effect was greater in MH muscle cells than in WT (Figure 2B). In WT incubation with OAG elevated $[Na^+]_i$ by 19% (from 8±0.1 mM, n=10 to 9.4±0.7 mM, n=9, p<0.001) in MH-HET by 42% (from 10±0.5 mM, n=10) to 14.2±0.7 mM, n=9, p<0.001) and in MH-HOM by 50% (from 13.9±0.5 mM, n=9 to 20.9±1.5 mM, n=10, p<0.001).

These elevations of $[Ca^{2+}]_i$ and $[Na^+]_i$ induced by OAG were not affected by the voltage gated Ca^{2+} channel inhibitor nifedipine (10 μM) nor associated with changes in resting membrane potential in either WT or MH muscle fibers (data not shown).

Removal of extracellular Ca^{2+} prevented $[Ca^{2+}]_i$ increases induced by OAG.

In a different set of experiments, we explored the contribution of the Ca^{2+} influx on $[Ca^{2+}]_i$ elevation elicited by OAG. Single WT and MH muscle fibers were incubated

for 5 min in Ca^{2+}-free solution prior to OAG (100μM) treatment. This exposure significantly reduced $[Ca^{2+}]_i$ in all genotypes but had a greater effect in MH than WT (Figure 3). In WT fibers Ca^{2+}-free solution reduced $[Ca^{2+}]_i$ from 123±4 nM (n=10) to 98±6 nM (n=12, p<0.001) while in MH-HET it was reduced from 161±26 nM (n=14) to 135±7 nM (n=12, p<0.001) and in MH-HOM from to 256±27 nM (n=12) to 176±17 nM (n=14, p<0.001). In addition, the observed rise in $[Ca^{2+}]_i$ elicited by OAG was completely inhibited in both WT and MH muscle fibers in the absence of extracellular Ca^{2+} (Figure 3).

Blocking sarcolemmal Ca^{2+} and Na^{+} entry with Gd^{3+} abolishes the increases in $[Ca^{2+}]_i$ and $[Na^{+}]_i$ elicited by OAG.

To gain further insight into molecular mechanisms for the increased sarcolemmal Ca^{2+} and Na^{+} entry responsible for the elevation in $[Ca^{2+}]_i$ and $[Na^{+}]_i$ after exposure to OAG, we measured $[Ca^{2+}]_i$ and $[Na^{+}]_i$ in isolated single WT and MH muscle fibers before and after incubation in Gd^{3+} and then in the presence of Gd^{3+}, after exposure to OAG (100μM). Pretreatment with Gd^{3+} (25 μM) significantly lowered $[Ca^{2+}]_i$ and $[Na^{+}]_i$ by 15% and by 8% respectively in WT by 20% by 15% respectively in MH-HET and by 27% and 29% respectively in MH-HOM (Figure 4A and B). Furthermore, Gd^{3+} pretreatment prevented any significant increase in $[Ca^{2+}]_i$ and $[Na^{+}]_i$ during exposure to OAG in all genotypes (Figure 4A and B).

SAR7334 blocks the effects of OAG.

Because Gd^{3+} is a non-specific sarcolemmal cation blocker, to further characterize the mechanism for the increase in $[Ca^{2+}]_i$ upon exposure to OAG, single WT and MH muscle fibers isolated were incubated in 1μM SAR7334, which is a new

more specific blocker of TRPC6 and TRPC3 channels[25] and then exposed to OAG (100μM). Pretreatment with SAR7334 significantly reduced the resting $[Ca^{2+}]_i$ by 14% in WT, 19% in MH-HET and 34% in MH-HOM, (Fig. 5A). Furthermore, SAR7334 also prevented the OAG-mediated elevation of $[Ca^{2+}]_i$ in all genotypes (Figure 5A).

SAR7334 partially blocked the elevation of $[Ca^{2+}]_i$ associated with MH episode

Having observed inhibition of the OAG-induced increase in $[Ca^{2+}]_i$ by SAR7334 in WT and MH single muscle fibers, we then tested the activity of this TRPC3/6 channel blocker during an MH episode. We, therefore, investigated the effect of SAR7334 on $[Ca^{2+}]_i$ in MH muscle *in vivo* during exposure to 2% halothane. $[Ca^{2+}]_i$ was measured simultaneously in the right and left *vastus lateralis* muscles in WT and MH-HOM mice before and after the addition of 2% halothane to their inspired gas (Insert Figure 4B). The right *vastus lateralis* muscle was pretreated locally with 1 μM SAR7334 and the left muscle served as the control. Figure 5B shows a typical *in vivo* experiment carried out in an MH-HOM mouse. Prior to drug treatment $[Ca^{2+}]_i$ was very similar in muscles from both legs (265±9 nM left leg *versus* 275±9 nM right leg). 10 min after the application of 1μM SAR7334 on the exposed *vastus lateralis* fibers of the right leg reduced $[Ca^{2+}]_i$ from 275±9 nM to 187±11 nM (Figure 5B). Inhalation of halothane elicited an elevation of $[Ca^{2+}]_i$ in the untreated leg to 1,373±81 nM while in the SAR7334-treated leg the initial increase in $[Ca^{2+}]_i$ was reduced by 62% (526±99 nM) after which $[Ca^{2+}]_i$ declined to 398±32nM (Figure 5B). After 20 min of inhalation of halothane, the rectal temperature reached 42º C, and the mouse died.

Hyperforin induced elevation of $[Ca^{2+}]_i$ and $[Na^{+}]_i$

Hyperforin is known to elevate the intracellular concentration of Ca^{2+} through the

activation of DAG-sensitive TRPC6 channels without activating the other TRPC isoforms (TRPC1, TRPC3, TRPC4, TRPC5, and TRPC7) [26]. Hyperforin (5 μM) caused a prominent sustained rise in $[Ca^{2+}]_i$, that was greater in MH (HOM>HET) than WT muscle fibers (Figure 6A). In WT muscle cells $[Ca^{2+}]_i$ was enhanced by 21% upon incubation with Hyperforin while in MH-HET it increased 43% and in MH-HOM by 64% (Figure 5A). Removal of extracellular Ca^{2+} reduced pre exposure $[Ca^{2+}]_i$ and blocked the hyperforin effect in all genotypes (Figure 6C). Similar to its effect on $[Ca^{2+}]_i$, hyperforin elevated $[Na^+]_i$ in WT from 8±01 mM (n=15) to 9.5±0.6 mM (n=10) (p<0.001), in MH-HET from 10±0.9 mM (n=15) (p<0.001) and in MH-HOM from 14.5±1.2 mM (n=11) to 20.3±1.6 mM (n=13) (p<0.001) (Figure 6B).

Effects of genotype and sarcolemmal cation entry agonists and antagonists on Mn^{2+} quench of Fura2 in differentiated myotubes

When the buffer was changed from imaging buffer to Mn^{2+} quench buffer baseline quench of Fura2 fluorescence was observed in all three genotypes (Figure 7A for representative traces) with the median quench rate being greater in MH-HOM (-0.229 AFU/s Interquartile range (IQR) -0.129 to -0.378 AFU/s) versus MH-HET(-0.184 AFU/s, IQR -0.105 to -0.32 AFU/s) and WT (-0.191 AFU/s, IQR -0.117 to -0.319 AFU/s) (Figure 7B).

Qualitatively similar results were observed in isolated adult single muscle fibers (data not shown).

We next determined the effect of sarcolemmal cation blockers 25 μM Gd^{3+} (a nonspecific sarcolemmal cation entry blocker), and 250 nM SAR7334 (a TRPC specific blocker) on the rate of Mn^{2+} quench of the fura2 fluorescence signal. Treatment with 25

μM Gd^{3+} profoundly blocked Mn^{2+} quench to near baseline levels in all three genotypes (p<0.0001, n=65 – 96, Figure 6B). The reduction in the median quench rate was 88% in WT (n=65), 100% in MH-HET (n=72) and 95.6% in MH-HOM (n= 96) (Figure 7B). After treatment with 250nM SAR7334 in WT cells the change in median quench rate was not significant (8%, p>0.999, n = 49), while MH-HET and in MH-HOM cells there was significant decrease (45%, p<0.005, n = 53 and 69%, p<0.001, n = 35 for MH-HET and MH-HOM respectively) in the median Mn^{2+} quench rate (Figure 7B).

Protein expression differences in WT and MH muscle.

Western blot analysis showed that TRPC3 and TRPC6 were significantly increased in a gene dose dependent manner in MH muscles (HET (p<0.01) and HOM (p<0.001) compared to WT. Figure 7A shows representative Western blot analysis of the expression of TRPC3 and TRPC6 in WT and MH-Het and MH-HOM muscle; ß actin was used as a loading control. Densitometric analysis of 5 independent Western blots for each TRPC protein is shown in Figure 7B.

Discussion.-

The major findings of the present study are as follows.

(1) We confirmed our previous finding[9] that *RYR1*-pG2435R muscle cells have chronically elevated intracellular resting $[Ca^{2+}]_i$ and $[Na^+]_i$ (HOM>HET) and now show that this is associated with elevated Mn^{2+} quench indicating increased sarcolemmal cation influx;

(2) Compared to WT, incubation of MH muscle cells with OAG or the TRPC6 activator hyperforin significantly increased $[Ca^{2+}]_i$ and $[Na^+]_i$ (HOM>HET);

(3) Increases in $[Ca^{2+}]_i$ and $[Na^+]_i$ induced by OAG are dependent on extracellular Ca^{2+} and are blocked by the nonspecific sarcolemmal cation channel blocker Gd^{3+};

(4) The OAG-induced increase in $[Ca^{2+}]_i$, and $[Na^+]_i$ could be blocked by the nonspecific sarcolemmal cation channel blocker Gd^{3+} as well as the specific TRPC3 and TRPC6 channel blocker SAR7334. SAR7334 treatment also significantly reduced resting $[Ca^{2+}]_i$ and $[Na^+]_i$, blocked Mn^{2+} quench, and reduced the elevation of $[Ca^{2+}]_i$ in MH fibers after exposure to halothane;

(5) The observed changes in the above *RYR1*-pG2434R responses were accompanied by an increase in the protein expression of TRPC3, TRPC6 in MH (HOM>HET) skeletal muscles compared to WT.

For some time it has been thought that the mechanism behind the increased resting $[Ca^{2+}]_i$ in MH susceptible muscle is simply due to SR leak and that the massive increase in muscle $[Ca^{2+}]_i$ during an MH episode comes from and is maintained by SR Ca^{2+} stores. Based on our studies in other MH animal models we have previously

suggested that sarcolemmal cation entry channels are at the very least, significant contributors to the chronically elevated $[Ca^{2+}]_i$ in quiescent MH muscles and myotubes[21-22] and that they play a similarly significant role during a fulminant MH episode[22].

A primary finding was that in addition to increased resting $[Ca^{2+}]_i$, resting $[Na^+]_i$ is also elevated in *RYR1*-pG2435R muscle cells (HOM>HET) compared to WT, both *in vitro* and *in vivo*[21-22]. This suggests that at least one source of Ca^{2+} could be the extracellular pool and not the SR. In this study we confirmed this hypothesis showing that incubation of muscle with Gd^{3+}, a potent non-specific inhibitor of sarcolemmal cation influx, significantly reduced the intracellular levels of both Na^+ and Ca^{2+} and blocked Mn^{2+} quench, a monitor of sarcolemmal cation entry.

DAG is a second messenger involved in key cellular processes in skeletal muscle and other excitable cells[27]. In addition to its role as a lipid second messenger to recruit protein kinases C, it also activates the DAG sensitive TRPC3/6 subgroup of TRPC channels which reside in the sarcolemma[24,28]. Here, for the first time in examining MH muscle cation homeostasis, we utilized the membrane-permeable DAG analogue, OAG to determine if the pathway for sarcolemmal Na^+ and Ca^{2+} influx was through TRPC3 and TRPC6[29]. OAG induced an elevation in the resting $[Ca^{2+}]_i$ and $[Na^+]_i$ in all three genotypes, and this was greater in MH (HOM>HET) muscle than WT (Figures 2A and 2B). The elevation of $[Ca^{2+}]_i$, and the increase in Mn^{2+} quench elicited by OAG was blocked either by removal of extracellular Ca^{2+} or by blocking sarcolemmal Ca^{2+} and Na^+ entry with Gd^{3+} or SAR7334 (Figures 3, 4 and 6). These data rule out any possibility that OAG increased $[Ca^{2+}]_i$ by releasing Ca^{2+} from intracellular stores, and confirmed that the

source of the increase was from the extracellular space through TRPC3/6 whose expression we showed was upregulated in MH compared to WT muscles.

Incubation of WT and MH single muscle fibers with SAR7334, a much more specific blocker of TRPC6 and TRPC3 channels than gadolinium[25], reduced resting $[Ca^{2+}]_i$ in MH cells (HOM<HET<WT) and blocked the effects of OAG on resting $[Ca^{2+}]_i$ and Mn^{2+} quench. Local application of SAR7334 directly to the superficial muscle fibers in vivo reduced resting $[Ca^{2+}]_i$ in MH-HOM fibers and partially inhibited the halothane-induced increase in $[Ca^{2+}]_i$ in MH muscle cells. This finding in particular demonstrates that during the MH episode there is an initial SR supported increase in $[Ca^{2+}]_i$ which soon appears to be quickly partially depleted, as demonstrated by the rapid fall in $[Ca^{2+}]_i$ from ~750nM to ~400nM in the SAR7334 treated leg during the same time $[Ca^{2+}]_i$ continues to increase to 1,373±81 nM and then plateaus in the non-treated leg. All of these data together support the hypothesis that sarcolemmal Ca^{2+} entry plays a critical role in maintaining the new $[Ca^{2+}]_i$ steady-state that has been observed during an MH crisis. Furthermore the observed immediate $[Ca^{2+}]_i$ elevation in the SAR7334 treated leg, is most probably mediated by the RyR1 Ca^{2+} release from the SR and the decline in the $[Ca^{2+}]_i$ in this leg shows that due to Ca^{2+} extrusion and blockade of sarcolemmal Ca^{2+} entry that this level cannot be maintained by SR Ca^{2+} cycling.

Consistent with the OAG-mediated elevation of $[Ca^{2+}]_i$ and $[Na^+]_i$ in muscle cells plus the ability of the TRPC specific blocker SAR7334 to block both the pharmacologic and halothane induced increases in Ca^{2+}, we also demonstrated that hyperforin, an activator of TRPC6 mediated inward cationic current[26,31,32], mimicked the action of OAG and its effect was greater in MH (HOM>HET) than WT muscle cells. As observed with

OAG activation removal of extracellular Ca^{2+} also eliminated the hyperforin-elicited increase in resting $[Ca^{2+}]_i$[31]. The enhanced cation flux observed across the sarcolemma in MH cells is consistent with the cell boundary theorem which states that the long term steady state of the free $[Ca^{2+}]_i$ inside cells must be driven by changes with the outside through fluxes across the plasmalemma[22,33].

In summary, these results demonstrated that mice expressing the *RYR1* mutation p.G2435R have an elevated resting skeletal muscle $[Ca^{2+}]_i$ and $[Na^+]_i$ and a significantly enhanced extracellular Ca^{2+} dependent response to OAG and a TRPC6 activator. We further showed that the OAG response could be prevented by TRPC3 and TRPC6 channel blockers. These results provide further support to our working hypothesis that in response to partial depletion of SR Ca^{2+} due to MH causing mutations in *RYR1*, TRPC3 and TRPC6 channels play a critical role in producing the intracellular Ca^{2+} and Na^+ overload both at rest and during the MH crisis.

References.-

1. Nelson TE: Malignant hyperthermia: a pharmacogenetic disease of Ca++ regulating proteins. Curr Mol Med 2002; 2: 347-69
2. Jurkat-Rott K, Lerche H, Lehmann-Horn F: Skeletal muscle channelopathies. J Neurol 2002; 249: 1493-502
3. Groom L, Muldoon SM, Tang ZZ, Brandom BW, Bayarsaikhan M, Bina S, Lee HS, Qiu X, Sambuughin N, Dirksen RT: Identical de novo mutation in the type 1 ryanodine receptor gene associated with fatal, stress-induced malignant hyperthermia in two unrelated families. Anesthesiology 2011; 115: 938-45
4. Parness J, Bandschapp O, Girard T: The myotonias and susceptibility to malignant hyperthermia. Anesth Analg 2009; 109: 1054-64
5. Litman RS, Rosenberg H: Malignant hyperthermia: update on susceptibility testing. JAMA 2005; 293: 2918-24
6. Robinson R, Carpenter D, Shaw MA, Halsall J, Hopkins P: Mutations in RYR1 in malignant hyperthermia and central core disease. Hum Mutat 2006; 27: 977-89
7. Yang T, Riehl J, Esteve E, Matthaei KI, Goth S, Allen PD, Pessah IN, Lopez JR: Pharmacologic and functional characterization of malignant hyperthermia in the R163C RyR1 knock-in mouse. Anesthesiology 2006; 105: 1164-75
8. Chelu MG, Goonasekera SA, Durham WJ, Tang W, Lueck JD, Riehl J, Pessah IN, Zhang P, Bhattacharjee MB, Dirksen RT, Hamilton SL: Heat- and anesthesia-induced malignant hyperthermia in an RyR1 knock-in mouse. FASEB J 2006; 20: 329-30
9. Lopez JR, Kaura V, Diggle CP, Hopkins PM, Allen PD: Malignant hyperthermia, environmental heat stress, and intracellular calcium dysregulation in a mouse model expressing the p.G2435R variant of RYR1. Br J Anaesth 2018; 121: 953-961
10. Du GG, Sandhu B, Khanna VK, Guo XH, MacLennan DH: Topology of the Ca2+ release channel of skeletal muscle sarcoplasmic reticulum (RyR1). Proc Natl Acad Sci U S A 2002; 99: 16725-30
11. Miller DM, Daly C, Aboelsaod EM, Gardner L, Hobson SJ, Riasat K, Shepherd S, Robinson RL, Bilmen JG, Gupta PK, Shaw MA, Hopkins PM: Genetic epidemiology of malignant hyperthermia in the UK. Br J Anaesth 2018; 121: 944-952
12. Robinson RL, Brooks C, Brown SL, Ellis FR, Halsall PJ, Quinnell RJ, Shaw MA, Hopkins PM: RYR1 mutations causing central core disease are associated with more severe malignant hyperthermia in vitro contracture test phenotypes. Hum Mutat 2002; 20: 88-97
13. Carpenter D, Robinson RL, Quinnell RJ, Ringrose C, Hogg M, Casson F, Booms P, Iles DE, Halsall PJ, Steele DS, Shaw MA, Hopkins PM: Genetic variation in RYR1 and malignant hyperthermia phenotypes. Br J Anaesth 2009; 103: 538-48
14. Lopez JR, Alamo L, Caputo C, DiPolo R, Vergara S: Determination of ionic calcium in frog skeletal muscle fibers. Biophys J 1983; 43: 1-4
15. Lopez JR, Alamo LA, Jones DE, Papp L, Allen PD, Gergely J, Sreter FA: [Ca2+]i in muscles of malignant hyperthermia susceptible pigs determined in vivo with Ca2+ selective microelectrodes. Muscle Nerve 1986; 9: 85-6

16. Yang T, Esteve E, Pessah IN, Molinski TF, Allen PD, Lopez JR: Elevated resting [Ca(2+)](i) in myotubes expressing malignant hyperthermia RyR1 cDNAs is partially restored by modulation of passive calcium leak from the SR. Am J Physiol Cell Physiol 2007; 292: C1591-8
17. Eltit JM, Bannister RA, Moua O, Altamirano F, Hopkins PM, Pessah IN, Molinski TF, Lopez JR, Beam KG, Allen PD: Malignant hyperthermia susceptibility arising from altered resting coupling between the skeletal muscle L-type Ca2+ channel and the type 1 ryanodine receptor. Proc Natl Acad Sci U S A 2012; 109: 7923-8
18. Feng W, Barrientos GC, Cherednichenko G, Yang T, Padilla IT, Truong K, Allen PD, Lopez JR, Pessah IN: Functional and biochemical properties of ryanodine receptor type 1 channels from heterozygous R163C malignant hyperthermia-susceptible mice. Mol Pharmacol 2011; 79: 420-31
19. Lopez JR, Allen PD, Alamo L, Jones D, Sreter FA: Myoplasmic free [Ca2+] during a malignant hyperthermia episode in swine. Muscle Nerve 1988; 11: 82-8
20. Yuen B, Boncompagni S, Feng W, Yang T, Lopez JR, Matthaei KI, Goth SR, Protasi F, Franzini-Armstrong C, Allen PD, Pessah IN: Mice expressing T4826I-RYR1 are viable but exhibit sex- and genotype-dependent susceptibility to malignant hyperthermia and muscle damage. FASEB J 2012; 26: 1311-22
21. Altamirano F, Eltit JM, Robin G, Linares N, Ding X, Pessah IN, Allen PD, Lopez JR: Ca2+ influx via the Na+/Ca2+ exchanger is enhanced in malignant hyperthermia skeletal muscle. J Biol Chem 2014; 289: 19180-90
22. Eltit JM, Ding X, Pessah IN, Allen PD, Lopez JR: Nonspecific sarcolemmal cation channels are critical for the pathogenesis of malignant hyperthermia. FASEB J 2013; 27: 991-1000
23. Yang T, Allen PD, Pessah IN, Lopez JR: Enhanced excitation-coupled calcium entry in myotubes is associated with expression of RyR1 malignant hyperthermia mutations. J Biol Chem 2007; 282: 37471-8
24. Hofmann T, Obukhov AG, Schaefer M, Harteneck C, Gudermann T, Schultz G: Direct activation of human TRPC6 and TRPC3 channels by diacylglycerol. Nature 1999; 397: 259-63
25. Maier T, Follmann M, Hessler G, Kleemann HW, Hachtel S, Fuchs B, Weissmann N, Linz W, Schmidt T, Lohn M, Schroeter K, Wang L, Rutten H, Strubing C: Discovery and pharmacological characterization of a novel potent inhibitor of diacylglycerol-sensitive TRPC cation channels. Br J Pharmacol 2015; 172: 3650-60
26. Leuner K, Kazanski V, Muller M, Essin K, Henke B, Gollasch M, Harteneck C, Muller WE: Hyperforin--a key constituent of St. John's wort specifically activates TRPC6 channels. FASEB J 2007; 21: 4101-11
27. Bouron A, Chauvet S, Dryer S, Rosado JA: Second Messenger-Operated Calcium Entry Through TRPC6. Adv Exp Med Biol 2016; 898: 201-49
28. Gudermann T, Hofmann T, Mederos y Schnitzler M, Dietrich A: Activation, subunit composition and physiological relevance of DAG-sensitive TRPC proteins. Novartis Found Symp 2004; 258: 103-18; discussion 118-22, 155-9, 263-6
29. Tu P, Kunert-Keil C, Lucke S, Brinkmeier H, Bouron A: Diacylglycerol analogues activate second messenger-operated calcium channels exhibiting TRPC-like properties in cortical neurons. J Neurochem 2009; 108: 126-38

30. Lemos VS, Poburko D, Liao CH, Cole WC, van Breemen C: Na+ entry via TRPC6 causes Ca2+ entry via NCX reversal in ATP stimulated smooth muscle cells. Biochem Biophys Res Commun 2007; 352: 130-4
31. Leuner K, Li W, Amaral MD, Rudolph S, Calfa G, Schuwald AM, Harteneck C, Inoue T, Pozzo-Miller L: Hyperforin modulates dendritic spine morphology in hippocampal pyramidal neurons by activating Ca(2+) -permeable TRPC6 channels. Hippocampus 2013; 23: 40-52
32. Treiber K, Singer A, Henke B, Muller WE: Hyperforin activates nonselective cation channels (NSCCs). Br J Pharmacol 2005; 145: 75-83
33. Rios E: The cell boundary theorem: a simple law of the control of cytosolic calcium concentration. J Physiol Sci 2010; 60: 81-4

Figure Legends.-

Figure 1. Elevated $[Ca^{2+}]_i$ and $[Na^+]_i$ in RyR1-G2435R MH muscle cells. $[Ca^{2+}]_i$ or $[Na^+]_i$ was measured in quiescent FDB fibers isolated from WT, MH-HET, and MH-HOM mice(**Fig. 1A**) and *in vivo* from the *vastus lateralis* fibers in anesthetized WT and MH mice (**Fig. 1B)** using double-barreled ion-specific microelectrodes. ***In vitro*** condition: n_{mice}= 3/experimental condition, n_{cell}= 15-18/genotype for $[Ca^{2+}]_i$; n_{mice}= 3/experimental condition, n_{cell} = 15-18/genotype for $[Na^+]_i$. ***In vivo*** condition: n_{mice}= 4/experimental condition, n_{cell} = 13-16/genotype for $[Ca^{2+}]_i$; n_{mice}= 5/experimental condition, n_{cell} = 8-11/ genotype for $[Na^+]_i$. Values are expressed as means ± S.D. for each condition. One-way ANOVA with Tukey's post-test, ***$p \leq 0.001$.

Figure 2. OAG provokes elevation of $[Ca^{2+}]_i$ and $[Na^+]_i$. Exposure of quiescent FDB fibers to 1-oleoyl-2-acetyl-sn-glycerol (OAG) 100 μM induced an elevation of $[Ca^{2+}]_i$ (**Fig. 2A**) and $[Na^+]_i$ (**Fig. 2B**) that was greater in MH (HOM>HET) than WT muscle fibers. Over the horizontal axis are indicated the experimental conditions used to measure $[Ca^{2+}]_i$ and $[Na^+]_i$. n_{mice}= 3/experimental condition, n_{cell}= 11-13/genotype for $[Ca^{2+}]_i$. n_{mice}= 3/experimental condition, n_{cell}= 9-10/genotype for $[Na^+]_i$. Values are expressed as means ± S.D. for each condition. One-way ANOVA with Tukey's post-test, ***$p \leq 0.001$.

Figure 3. Removal of $[Ca^{2+}]_e$ prevents the OAG-induced increase in $[Ca^{2+}]_i$. Removal of extracellular Ca^{2+} lowered the $[Ca^{2+}]_i$ and provoked the inhibition of OAG (100 μM)-induced elevation of $[Ca^{2+}]_i$ in FDB fibers isolated from WT, MH-HET, and MH-HOM mice. On the horizontal axis are indicated the experimental conditions used to measure $[Ca^{2+}]_i$. n_{mice}= 3/experimental condition, n_{cell}= 10-14/genotype for $[Ca^{2+}]_i$. Values are expressed as means ± S.D. for each condition. One-way ANOVA with Tukey's post-test, ***$p \leq 0.001$.

Figure 4. Gd^{3+} abolishes the OAG effects on $[Ca^{2+}]_i$ and $[Na^+]_i$. Preincubation of WT, MH-HET, and MH-HOM FDB fibers in Gd^{3+} (25 μM) reduced the $[Ca^{2+}]_i$ and $[Na^+]_i$ and eliminated the increase in $[Ca^{2+}]_i$ **(Fig. 4A)** and $[Na^+]_i$ **(Fig. 4B)** induced by OAG. Over the horizontal axis are indicated the experimental conditions used to measure $[Ca^{2+}]_i$ and $[Na^+]_i$. n_{mice}= 4/experimental condition, n_{cell}= 17-19/genotype for $[Ca^{2+}]_i$. n_{mice}= 4/experimental condition, n_{cell}= 13-15/genotype for $[Na^+]_i$. Values are expressed as means ± S.D. for each condition. One-way ANOVA with Tukey's post-test, ***$p \leq 0.001$.

Figure 5. SAR7334 blocked the elevation of $[Ca^{2+}]_i$ induced by OAG and partially inhibits the increase associated with an MH episode. $[Ca^{2+}]_i$ was measured WT, MH-HET, and MH-HOM FDB fibers before and after incubation in SAR7374 (1μM), as well as after the exposure with SAR7374 and OAG (100 μM). **Fig. 5A** shows that preincubation in SAR7374 reduced $[Ca^{2+}]_i$ in all genotypes and prevent the increase in intracellular calcium concentration induced by OAG. Over the horizontal axis are indicated the experimental conditions used to measure $[Ca^{2+}]_i$. **Fig. 5B** shows a typical experiment carried out *in vivo* in anesthetized (ketamine/xylazine) MH-HOM mice. $[Ca^{2+}]_i$ was measured simultaneously on the superficial fibers of the *vastus*

lateralis muscle in the right and left hind mice. Superficial muscle fibers were perfused with Ringer solution alone (left leg, control, red line) or SAR7374 (1µM) for 5 min (right leg, black line) and then the mouse was exposed to inhaled halothane 2% (black arrow). The insert on the left upper corner shows the experimental arrangement: *1* and *2* calcium microelectrodes, *3* and *4* grounds, *5* rectal temperature probe. For $[Ca^{2+}]_i$ in **Fig.5A**: n_{mice}= 4/experimental condition, n_{cell}= 18-13/genotype. For $[Ca^{2+}]_i$ in **Fig.5B**: n_{mice}= 7. Values are expressed as means ± S.D. for each condition. One-way ANOVA with Tukey's post-test, ***$p \leq 0.001$.

Figure 6. Effect of hyperforin on $[Ca^{2+}]_i$. Hyperforin (5 µM) caused a sustained rise in $[Ca^{2+}]_i$ and $[Na^+]_i$ in single muscle fibers that were greater in MH (HOM>HET) than WT (**Fig. 6A and 6B**). Removal of extracellular Ca^{2+} inhibited the hyperforin effect on $[Ca^{2+}]_i$ ***(Fig. 6C).*** On the horizontal axis are indicated the experimental conditions. For $[Ca^{2+}]_i$ in **Fig. 6A**: n_{mice}= 3/experimental condition, n_{cell}= 9/10 genotype. For $[Na^+]_i$ in **Fig. 6B**: n_{mice}= 3/experimental condition, n_{cell}= 15/10 genotype. For $[Ca^{2+}]_i$ in **Fig. 6C**: n_{mice}= 3/experimental condition, n_{cell}= 12/10 genotype. Values are expressed as means ± S.D. for each condition. Paired and unpaired *t*-test and one-way ANOVA with Tukey's post-test, ***$p \leq 0.001$.

Figure 7: Resting sarcolemmal divalent cation permeability in myotubes. (A) Representative traces indicating the change in the rate of the fura2 fluorescence that was quenched by Mn^{2+} in WT, MH-HET and HOM myotubes from RyR1-G2435R mice upon changing from IB to MnB. **(B)** Box-plots showing the quench rate (median±Inter Quartile Range) in control, 25 µM Gd^{3+} or 250 nM SAR7334 treated myotubes from each of the three genotypes. The whiskers represent the 10-90th centile. A larger rate of quench is represented by a more negative number and this indicates a greater cationic entry through the sarcolemmal cation channels into the cell from the extracellular space which is an estimate of the sarcolemmal permeability to Ca^{2+}. $p<0.05$ in MH-HOM versus MH-HET and WT. **$p<0.005$ and $p<0.0001$ in each genotype *vs.* their control conditions (Kruskall-Wallis test with Dunn's multiple comparisons test, n≥35 myotubes for each condition).

Figure 8. Fig. 8A shows representative Western blots showing the expression of TRPC3, TRPC6 and ß-actin in WT, MH-HET and MH-HOM gastrocnemius muscles. Densitometric analysis of 5 independent Western blots for each TRPC protein is shown in **Fig. 8B**. Data were normalized to ß-actin and are expressed as mean ± S.D. n_{mice}=4. Paired *t*-test, ** $p \leq 0.01$, ***$p \leq 0.001$

Tables: Not Applicable

Appendices: Not Applicable

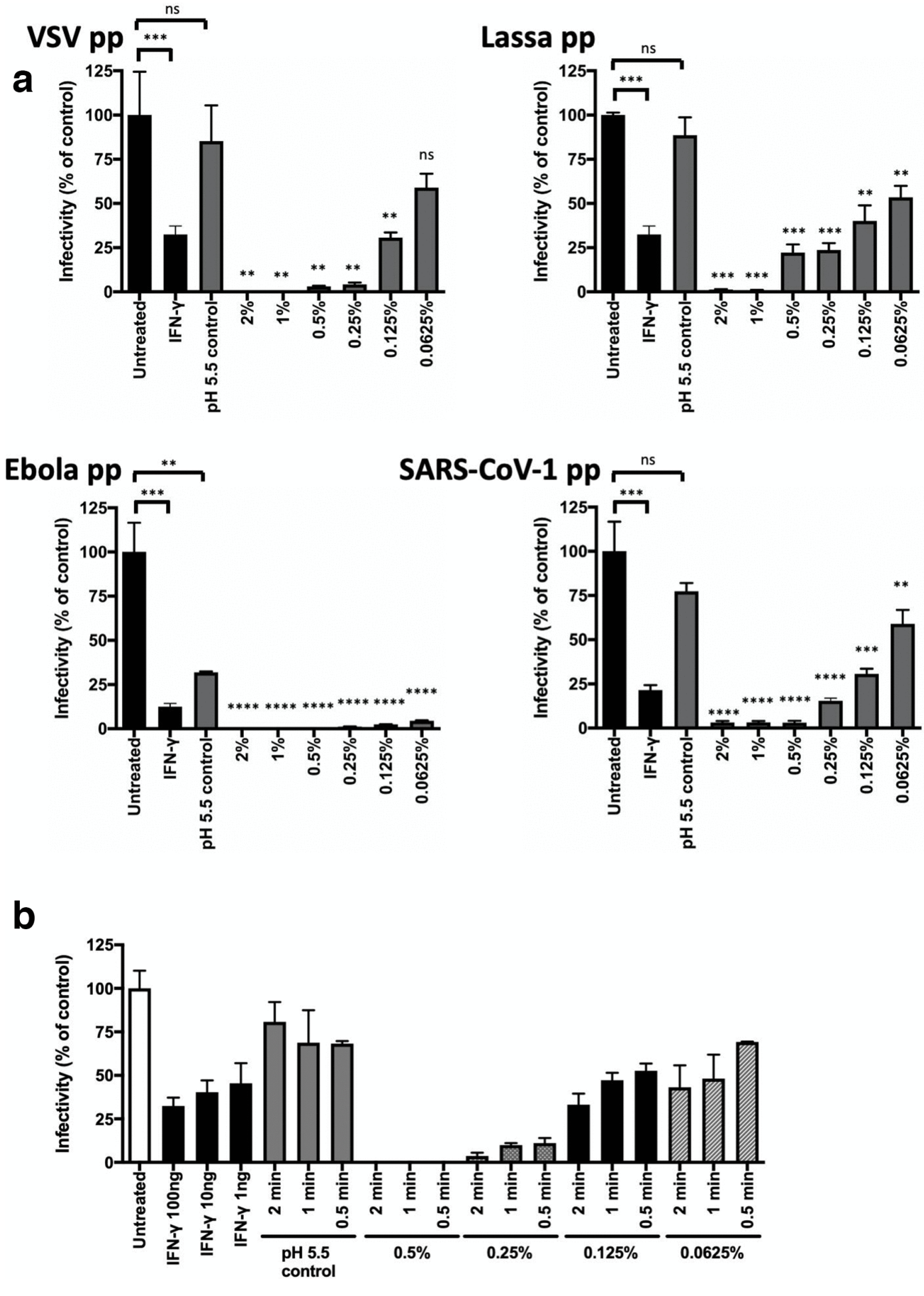
a
VSV pp
Lassa pp
Ebola pp
SARS-CoV-1 pp
Infectivity (% of control)
Untreated
IFN-γ
pH 5.5 control
2%
1%
0.5%
0.25%
0.125%
0.0625%
ns
b
IFN-γ 100ng
IFN-γ 10ng
IFN-γ 1ng
2 min
1 min
0.5 min
pH 5.5 control
0.5%
0.25%
0.125%
0.0625%

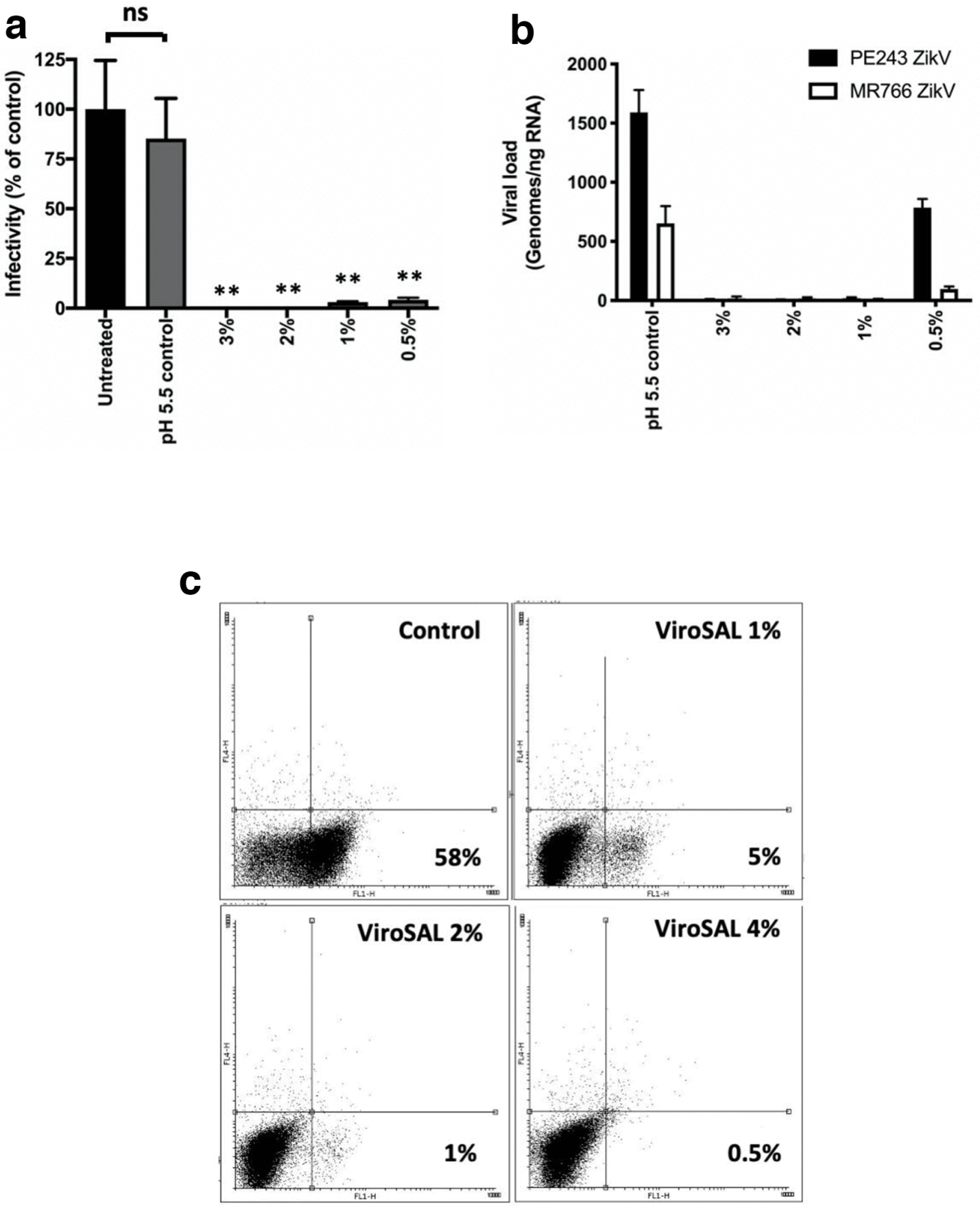
a
ns
Infectivity (% of control)
125
100
75
50
25
0
**
**
**
**
Untreated
pH 5.5 control
3%
2%
1%
0.5%
b
PE243 ZikV
MR766 ZikV
Viral load
(Genomes/ng RNA)
2000
1500
1000
500
0
pH 5.5 control
3%
2%
1%
0.5%
c
Control
58%
ViroSAL 1%
5%
ViroSAL 2%
1%
ViroSAL 4%
0.5%
FL4-H
FL1-H

a

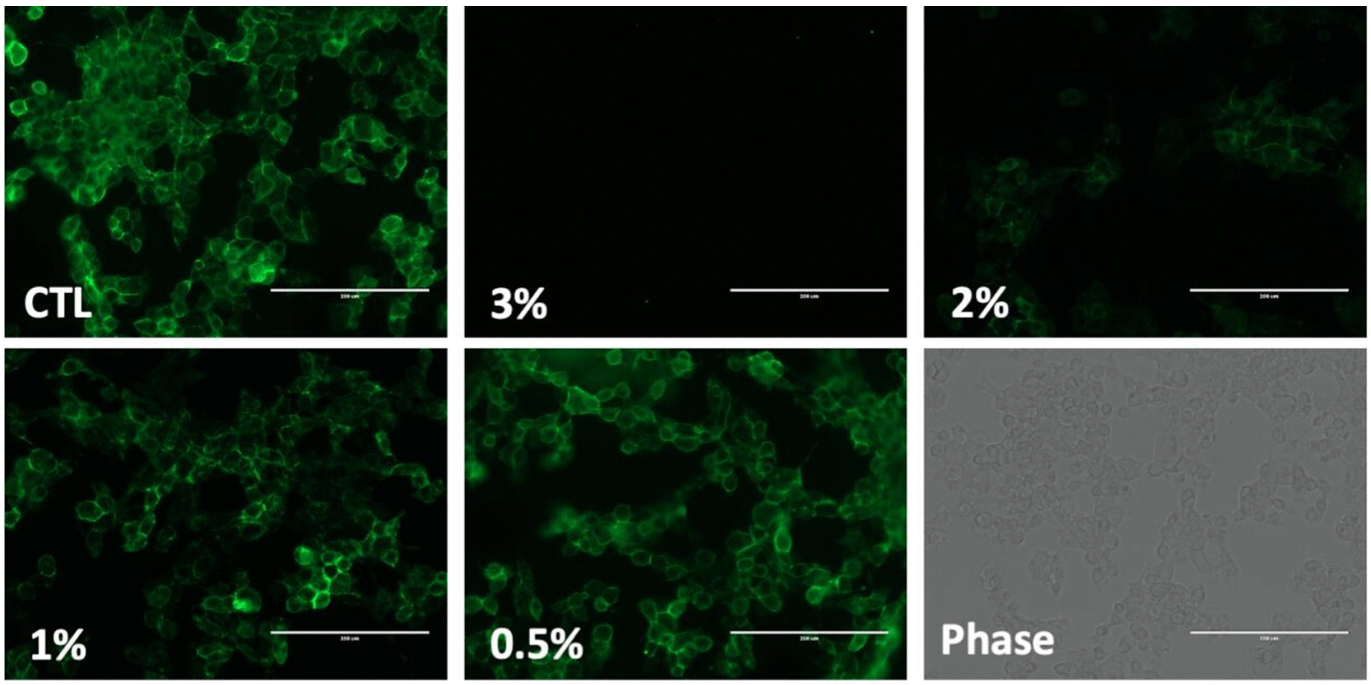
CTL
3%
2%
1%
0.5%
Phase

b

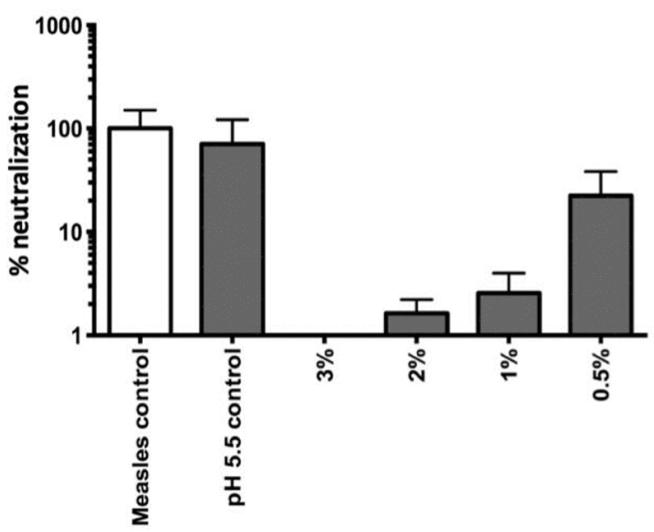
% neutralization
1000
100
10
1
Measles control
pH 5.5 control
3%
2%
1%
0.5%

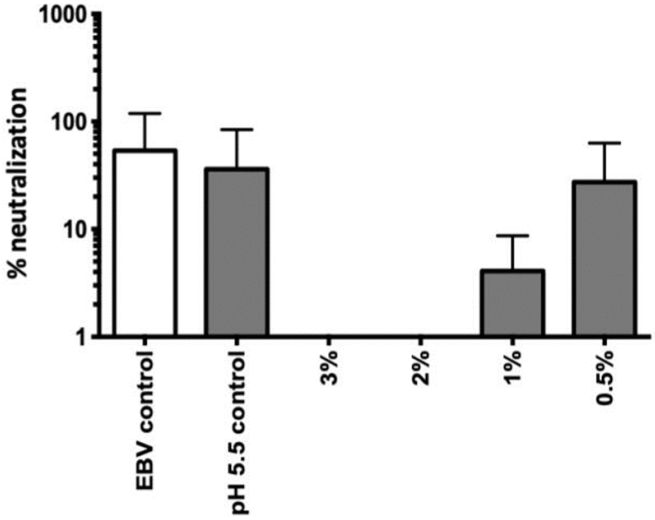
% neutralization
1000
100
10
1
EBV control
pH 5.5 control
3%
2%
1%
0.5%

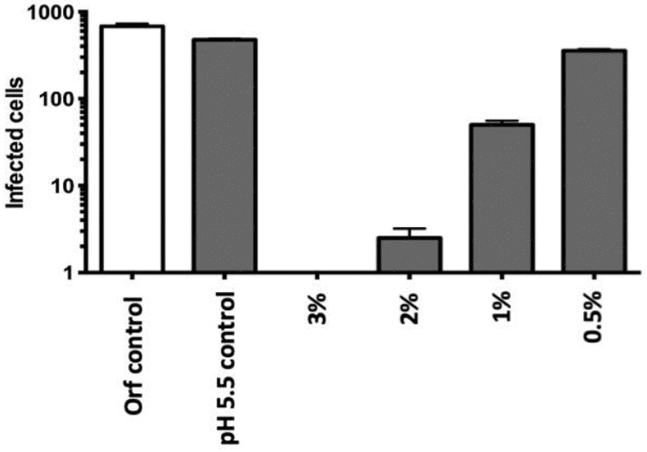
Infected cells
1000
100
10
1
Orf control
pH 5.5 control
3%
2%
1%
0.5%

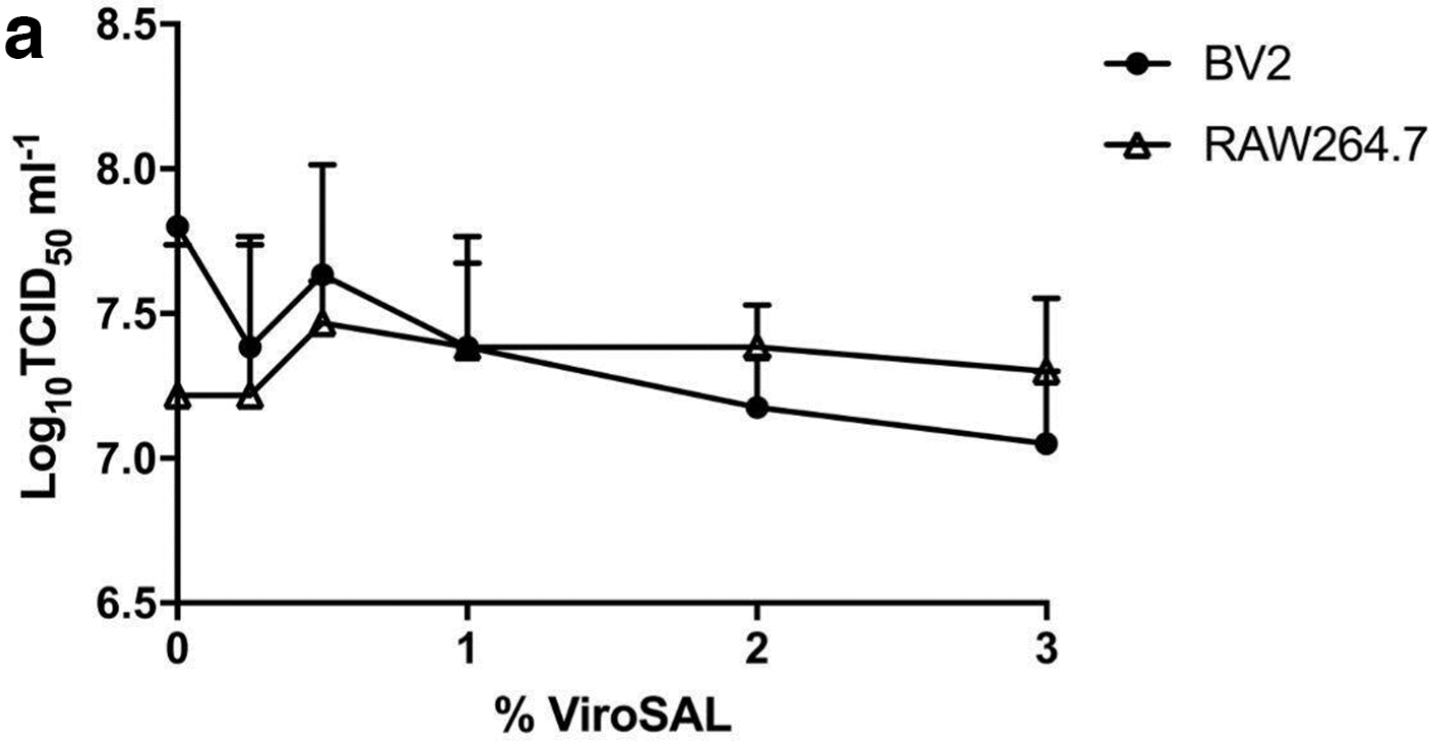
a
8.5
8.0
7.5
7.0
6.5
Log10TCID50 ml-1
0
1
2
3
% ViroSAL
BV2
RAW264.7

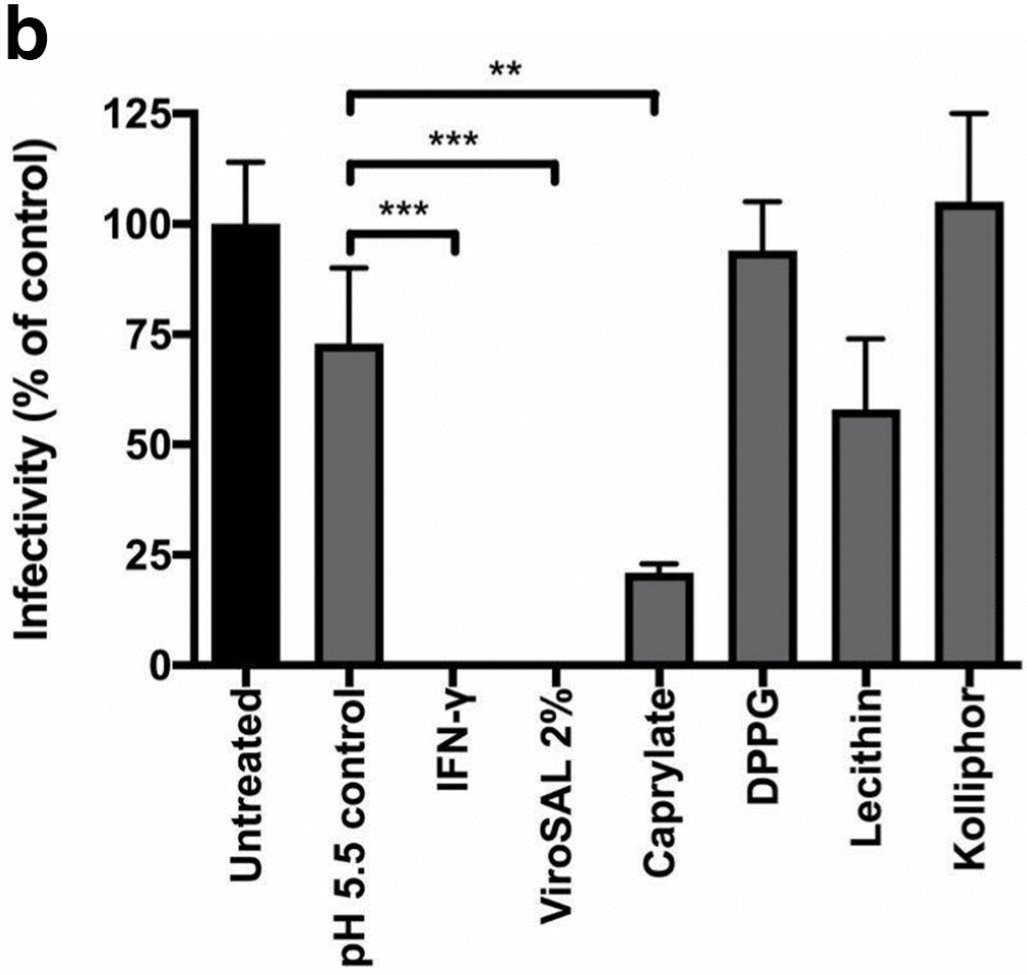
b
125
100
75
50
25
0
Infectivity (% of control)
**
***
***
Untreated
pH 5.5 control
IFN-γ
ViroSAL 2%
Caprylate
DPPG
Lecithin
Kolliphor

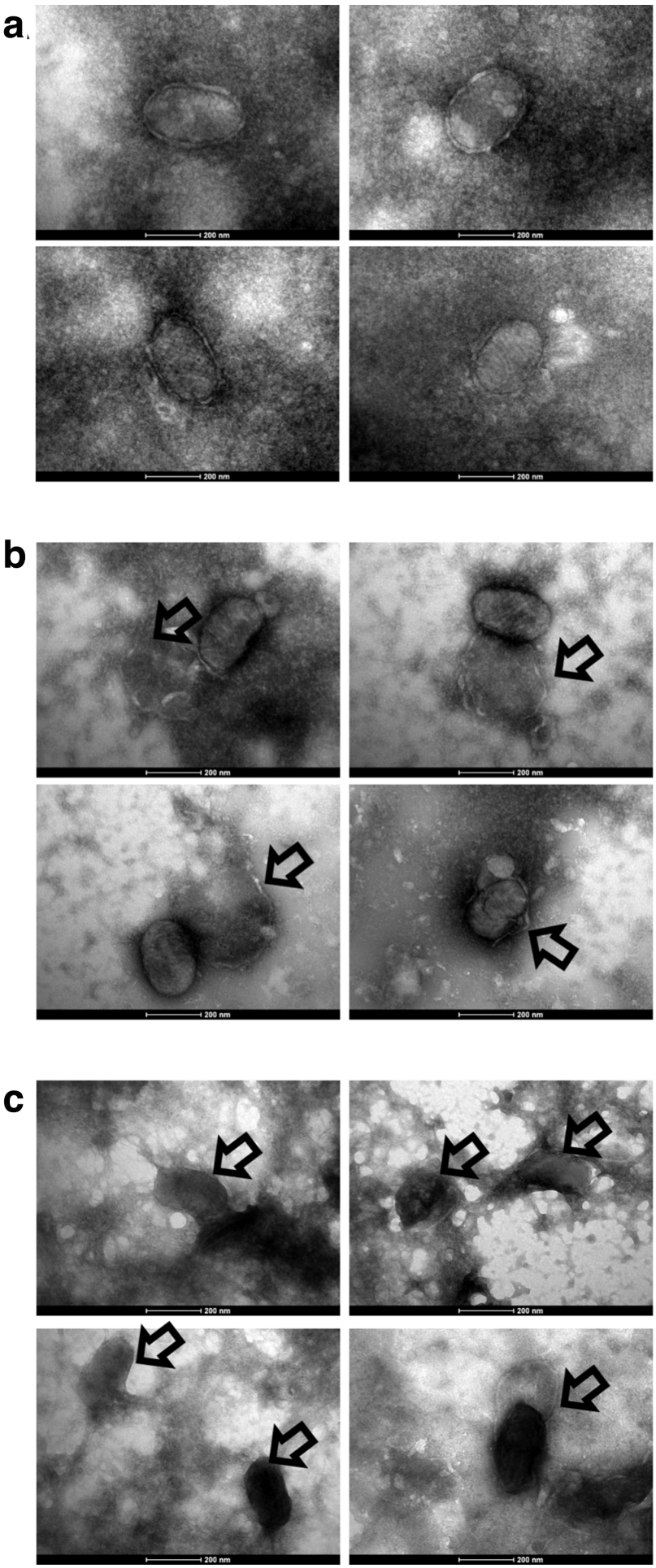
a
200 nm
200 nm
200 nm
200 nm
b
200 nm
200 nm
200 nm
200 nm
c
200 nm
200 nm
200 nm
200 nm

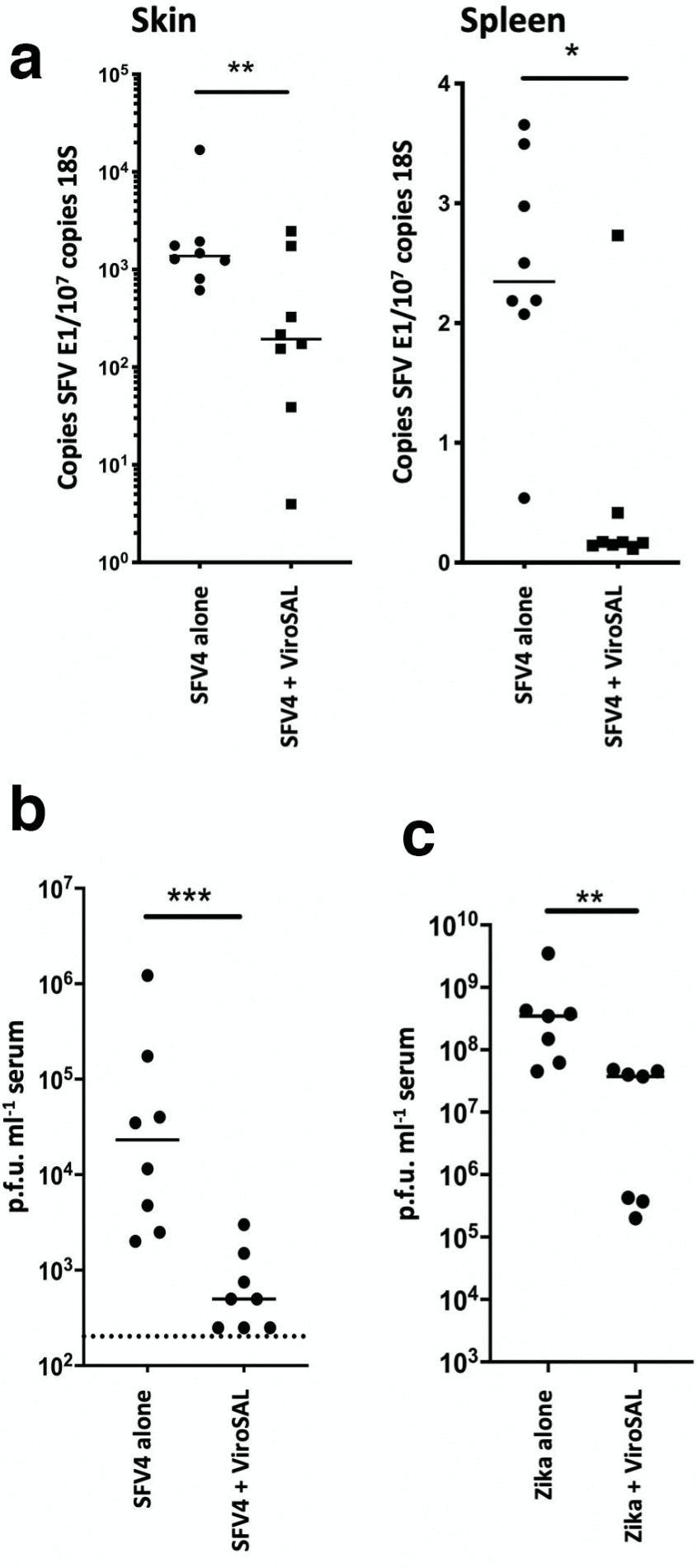
a
Skin
Spleen
Copies SFV E1/10^7 copies 18S
**
*
SFV4 alone
SFV4 + ViroSAL
b
p.f.u. ml-1 serum
***
SFV4 alone
SFV4 + ViroSAL
c
p.f.u. ml-1 serum
**
Zika alone
Zika + ViroSAL